Published in final edited form as:
Biochim Biophys Acta. 2010 August ; 1800(8): 834–845. doi:10.1016/j.bbagen.2009.12.005.

The Ferritin Superfamily: Supramolecular Templates for Materials Synthesis

Masaki Uchida[1,2], **Sebyung Kang**[1,2], **Courtney Reichhardt**[1,2], **Kevin Harlen**[1,2], and **Trevor Douglas**[*,1,2]

[1]Department of Chemistry and Biochemistry, Montana State University, Bozeman, MT 59717

[2]Center for Bioinspired Nanomaterials, Montana State University, Bozeman, MT 59717

Abstract

Members of the ferritin superfamily are multi-subunit cage-like proteins with a hollow interior cavity. These proteins possess three distinct surfaces, i.e. interior and exterior surfaces of the cages and interface between subunits. The interior cavity provides a unique reaction environment in which the interior reaction is separated from the external environment. In biology the cavity is utilized for sequestration of irons and biomineralization as a mechanism to render Fe inert and sequester it from the external environment. Material scientists have been inspired by this system and exploited a range of ferritin superfamily proteins as supramolecular templates to encapsulate nanoparticles and/or as well-defined building blocks for fabrication of higher order assembly. Besides the interior cavity, the exterior surface of the protein cages can be modified without altering the interior characteristics. This allows us to deliver the protein cages to a targeted tissue *in vivo* or to achieve controlled assembly on a solid substrate to fabricate higher order structures. Furthermore, the interface between subunits is utilized for manipulating chimeric self-assembly of the protein cages and in the generation of symmetry-broken Janus particles. Utilizing these ideas, the ferritin superfamily has been exploited for development of a broad range of materials with applications from biomedicine to electronics.

Keywords

Ferritin; Dps (DNA binding protein from nutrient starved cells); Nanoparticle; Multi-functionalities; Biomimetic chemistry; Janus particle; Bio-template

Introduction

The interaction between hard (inorganic) and soft (organic) materials in biomineralization provides the basis for controlled morphology, polymorph selection, and spatial localization in biological systems. Understanding the basis for these interactions has been significant in the design and implementation of synthetic biomimetic systems.

[*]To whom correspondence should be addressed, address: CBB 113, Montana State University, Bozeman, MT 59717, tdouglas@chemistry.montana.edu, Tel: (406) 994-6566, Fax: (406) 994-5407.

The iron storage protein ferritin is a unique biomineralization system and is the inspiration for the work described below. It is an apparently simple system with only a single protein component, which directs biomineralization of iron oxide at the protein-solution interface. The protein forms a closed shell architecture (Figure 1), which incorporates all the control elements necessary for biomineralization. These elements include an enzymatic catalyst for molecular transformation of precursor ions, a mineral nucleation site, and an architecture that defines and constrains the overall morphology of the biomineral. Additionally, the colloidal nature of the protein cage renders the final biomineral soluble and mobile, yet biochemically inert. Many of these properties and control elementsare highly desired in the fabrication of synthetic materials, and we (and others) have incorporated some of our understanding of the ferritin biomineralization towards biomimetic synthesis.

Supramolecular assemblies of protein subunits into cage-like architectures are not unique to ferritins, and from a synthetic biomimetic standpoint such assemblies represent novel environments by which materials can be synthesized in a size-constrained mode of encapsulation. There are a number of protein cage architectures that, like ferritin, assemble from a distinct number of subunits to form a precisely defined molecular container in the 5-100 nm size regime. Examples of these cage-like architectures are chaperonins[1-3], DNA binding proteins[4-9], and a very large class of protein cages-namely viruses[10, 11]. Typically, protein cages are roughly spherical in nature and represent a range of relatively simple symmetries including tetrahedral, octahedral, and icosahedral. The library of functional protein cage architectures that serve as platforms for such purposes as biomimetic material synthesis, magnetic resonance imaging (MRI) contrast agents, gene therapy, drug encapsulation, cell specific targeting and catalysis is being developed.

Conceptually, there are three unique interfaces presented by these protein cage architectures, the interior and exterior surfaces as well as the interface between subunits (Figure 2). Here we present two particular protein cage platforms, ferritin and Dps (DNA binding protein from nutrient starved cells), that serve as size-constrained reaction vessels for nano-material synthesis, specifically exploiting the *interior* surface of the protein cage. The exterior surface has been utilized for targeting and the subunit interface has been used to direct the assembly of chimeric and symmetry-broken architectures. From the understanding of directed biomineralization in ferritin, we have developed a model for surface-induced metal oxide formation and used this as a guiding principle for the synthesis of metal oxide nano-particles in other, natural and engineered, protein cage architectures. In this way, we have demonstrated control over composition, polymorph selection, and overall morphology using synthetic reactions. The principles outlined here are not limited to the two protein cage systems described, but rather serve as a model for protein encapsulated biomimetic synthesis [12].

Mineralization of Ferritin and Dps Proteins

Biomineralization of iron oxide in mammalian ferritin

Ferritin (Fn) is a spherical protein cage architecture that is nearly ubiquitous in biology where it functions to direct the biomineralization of iron as a mechanism for maintaining iron homeostasis [13, 14]. While the primary amino acid sequences of ferritins show little homology, the structural homology (at the 2°, 3°, and 4° levels) is highly conserved. All ferritins are composed of 24 structurally identical subunits that assemble into a very robust protein cage with octahedral (432) symmetry (Figure 1). The external diameter of these assembled protein cages is 12 nm and the internal cavity is 6-8 nm in diameter. The structural motif of the ferritin subunit consists of a four-helix bundle with a fifth C-terminal helix (helix E) oriented at 60° to the four-helix bundle axis. In the 4° structure of the

assembled protein cage the fifth helix forms the four fold axis through assembly of an intersubunit four-helix bundle[15-17].

Mammalian ferritin is comprised of two classes of subunits that are nearly structurally identical, although they differ in 1° sequence. These two forms of subunits, H-chain (heavy) and L-chain (light), self assemble to form hetero-24mers with different ratios of each subunit depending upon the organ from which the ferritin is isolated. The designations of H and L were made based on their differences in subunit electrophoretic mobility with molecular masses of 21 and 19 kDa respectively [13]. H-chain ferritin has a conserved enzymatic activity known as the ferroxidase site and is known to catalyze the oxidation of Fe^{2+}, with molecular O_2, more rapidly than L-chain. L-chain subunit has a greater negative charge, which in the assembled Fn is presented on the interior surface as clusters of acidic residues (Glu and Asp) that comprise the mineral nucleation site. H-chain ferritin also has a nucleation site that is in close proximity to the ferroxidase site with one glutamate residue shared between the two sites[15].

While iron is a necessary element for life, it has a paradoxical relationship in biology due to its reactivity in forming reactive oxygen species. When iron is stored as a nano-particle of iron oxide (ferrihydrite) inside the ferritin protein cage, it is completely sequestered and rendered inert[18]. The encapsulation and sequestration of the iron oxide nano-particle in biological systems highlights its potential for use as a synthetic platform for materials synthesis. The cage-like property of ferritin provides an ideal size-constrained reaction environment for nano-material synthesis with the protein shell acting both to direct mineralization and as a passivating layer, preventing unwanted particle-particle interactions.

Mineralization

In vivo, ferritin is responsible for sequestering and storing toxic iron as an innocuous mineral of iron oxide through an overall protein mediated reaction represented in Reaction 1 [18].

$$4Fe^{2+}+O_2+6H_2O \rightarrow 4Fe(O)OH+8H^+ \quad (1)$$

The actual biological process of iron oxidation and encapsulation is considerably more complex than Reaction 1 indicates and some of the intimate steps remain unresolved. The mineralized iron particles are electron dense and are the approximate dimensions of the interior of the protein cage (5-7 nm diameter). When iron is allowed to undergo oxidative hydrolysis *in vitro* in the absence of Fn, an uncontrolled homogeneous nucleation results in mineralization and precipitation of iron oxide. There are approximately fifteen common polymorphs of iron oxide or iron oxy-hydroxide[19] but under the narrow range of conditions compatible with biology, and in the absence of macromolecular directing agents the mineral phases of lepidocrocite (γ-FeO(OH)) or goethite (α-FeO(OH)) will be formed [13]. It is interesting to note that in the presence of Fn, only a particular phase of iron oxide (ferrihydrite) is formed. Ferrihydrite is less crystalline than lepidocrocite or goethite and is characterized by electron or X-ray diffraction studies to commonly have either two or six diffraction lines but has recently been structurally characterized using pair distribution function anlysis[20]. This kinetically trapped phase of iron oxide is not usually a particularly stable phase but is stable when prepared inside Fn, indicating the ability of biomolecules to direct and selectively stabilize a particular polymorph.

The mechanism by which iron is incorporated into Fn *in vitro* can be described by four major events: iron entry, iron oxidation, iron oxide nucleation, and iron oxide particle growth. The multi-step mineralization process is mediated at all levels by the protein cage.

Iron entry into the cage-like architecture occurs via the channel (3-fold symmetry) formed at the interface between subunits [21, 22]. Fe^{2+} oxidation is enzymatically catalyzed by reaction at the ferroxidase center resulting in the formation of Fe^{3+}. The nucleation of an iron oxide material from this insoluble ion is facilitated at the interior protein surface, and the particle grows from this nucleus but is limited by the size constraints of the cage.

The iron oxide mineralization processes in mammalian ferritin can be summarized by a series of reactions (Reactions 2-6) which results in the formation of a spatially constrained iron oxide nano-particle core[23].

$$P+2Fe^{2+} \rightarrow P[Fe_2]^{4+} \quad (2)$$

$$P[Fe_2]^{4+}+O_2 \rightarrow P[Fe_2O_2]^{4+} \quad (3)$$

$$P[Fe_2O_2]^{4+} \rightarrow P[Fe_2^{6+}O_2^{2-}]^{4+} \quad (4)$$

$$P[Fe_2^{6+}O_2^{2-}]^{4+}+H_2O \rightarrow P[Fe_2O]^{4+}H_2O_2 \quad (5)$$

$$P[Fe_2O]^{4+}+H_2O \rightarrow P+2Fe(O)OH+2H^{+} \quad (6)$$

In this scheme P is the protein and the presence of either hydroxide ions or bound glutamate residues of the protein balance the charge. Reaction 2 demonstrates initial binding of two Fe^{2+} to the protein cage (at the ferroxidase center); Reaction 3 is the binding of molecular O_2 to form a dioxygen complex; Reaction 4 is the oxidation of the di-ferrous complex to form the differic complex; Reaction 5 is the formation of the peroxo intermediate followed by degradation to the m-oxo-bridged complex; and Reaction 6 is the release of the iron complex from the ferroxidase site to form the FeOOH core at the nucleation site [23]. This mechanism leads to the overall reaction presented in the balanced Reaction 1.

The ferroxidase reaction suggests that ferritin biomineralization is specific for iron *in vivo*. However, *in vitro* experiments with homopolymers of L-chain Fn, having no ferroxidase activity, have been shown to encapsulate iron oxide nano-particles at nearly equivalent efficiencies [24]. H-ferritin mutants, where the nucleation sites have been deleted but the ferroxidase sites remain intact, are also able to spatially direct mineralization within the confines of the protein cage. In mutant L-ferritins, lacking both the ferroxidase and the nucleation sites, there was a loss of spatial control in directing mineral formation and bulk precipitation of iron oxides occurred[24, 25]. What then are the roles of the ferroxidase and nucleation sites that make them individually dispensable but together an absolute requirement? The ferroxidase site converts Fe^{2+} to Fe^{3+}. The Fe^{2+} is orders of magnitude more soluble, at physiologically relevant pH, than the Fe^{3+}. Thus, the ferroxidase center converts an under saturated condition to a supersaturated condition *inside the protein cage* – this is sufficient to achieve the spatially directed mineralization observed. The high negative charge density on the interior surface of the assembled Fn protein cage that constitutes the nucleation sites serves to aggregate ions at the protein interface, which may increase the local concentration of ions at the interface and facilitate oxidative mineralization. Each of these components is sufficient to direct mineralization, but when they are both absent, all control is removed.

Model for synthetic nucleation driven mineralization

Observing successful nucleation site driven mineralization in ferritin suggests that the oxidation and mineralization reaction may not exhibit a high degree of specificity for iron, and that mineralization could be expected to occur for a range of transition metal ions. The data indicates that iron mineralization can be driven through purely electrostatic effects at the interior protein interface. A model for this activity can be approximated using Gouy-Chapman theory of charged surfaces. Briefly, Gouy-Chapman theory states that the charge on a surface influences the ion distribution of electrolytes proximally to the surface through Coulombic interactions (Figure 3)[26, 27]. The surface charge potential decays exponentially as a function of distance from surface according to Equation 7.

$$\psi_x = \psi_0 e^{-kx} \quad (7)$$

Where Ψ_x is the potential at a distance x, Ψ_0 is the surface potential, and κ is a Debye parameter measured in reciprocal distance. The distance (x) from the surface where Ψ_x is (1/e) Ψ_0 defines the thickness of the diffuse double layer. The width of the double layer changes as a function of ionic strength of the media and the charge of the interacting ion. This distance can be determined using Equation 8, which determines the electric potential profile of the diffuse double layer.

$$\kappa = \left(\frac{e^2 \sum n_i^0 z_i^2}{\epsilon_0 \epsilon_\gamma k_B T}\right)^{1/2} \quad (8)$$

In Equation 8, e is the fundamental charge (C), n_i is the ionic strength, z_i is the charge of the interacting ion, e_0 is the dielectric constant of the solution, e_g is the permittivity in a vacuum, k_B is Boltzmann's constant, and T is absolute temperature[28]. Assuming an ionic strength of approximately 0.1 M, the thickness of the diffuse double layer for divalent cations (Fe^{2+}, Co^{2+}, Mn^{2+} etc.) is 0.758 nm, and for a trivalent cation is 0.339 nm. The exponential decay of the surface potential with distance is illustrated in Figure 3. The concentration of counterions follows the surface potential and exhibits maximal concentration at the interface but drops off exponentially and approaches bulk concentration a few nanometers from the surface. For divalent metal species the potential Ψ_x drops to 10% of the surface potential Ψ_0 within 1.74 nm of the surface of the cage, and 0.78 nm for trivalent metal species. According to this model, the very negatively charged interior surface of Fn will accumulate counter ions (Fe^{2+}), at concentrations significantly higher than bulk concentration, in close proximity to this surface. This could potentially have two effects, both of which facilitate the oxidative mineralization process that results in the formation of the iron oxide core in ferritin. The first is that binding of Fe^{2+} to negatively charged carboxyl species greatly lowers the reduction potential making oxidation a favorable process. Since the nucleation sites in ferritin are comprised of clusters of glutamic acid residues, accumulation of Fe^{2+} at this interface is expected to increase the oxidation of Fe^{2+} to form Fe^{3+}. Secondly, the highly charged surface which accommodates the accumulation of $Fe^{2+/3+}$ ions in close proximity acts as a substrate for stabilizing highly charged clusters; the precursors of the nucleation site of L-chain Fn consists of residues E57, E60, E61, E64 and E67, all of which reside on or close to the interior surface of the protein [25]. This model for surface charge directed oxidative mineralization suggests that there is very little specificity for iron. In biological systems the iron specificity most probably arises from the specific transport of iron to ferritin, as there is almost certainly no free iron in the cell. The lack of specificity for iron has, however, been used very successfully for directing the

formation of other metal oxide particles in ferritin and other protein cage architectures as described in later sections.

Protein cage directed mineralization appears to require three essential features: 1) channels in the protein shell that allow molecular access to the interior the protein cage from the bulk solution; 2) chemically distinct interior and exterior surfaces; and 3) protein cage stability under the conditions required for the synthesis. This model has provided a rational approach for synthetic biomimetic mineralization that relies on the electrostatic character of the interior of a protein cage for directing material synthesis.

Dps – a 12 Subunit protein cage

In order to test the electrostatic model for protein directed mineralization, synthetic reactions were performed using a protein cage, Dps, with characteristics similar to Fn but without the clear biological mineralization function of ferritin. There is a clear relationship between Fn and the Dps proteins – they are both members of the ferritin superfamily. Dps was originally isolated from *E. coli*[29], and since its discovery structural and functional homologues have been isolated in many other bacteria [30-32] as well as archaea [7, 8, 33]. While there is some structural similarity between Fn and Dps proteins, the Dps protein cage is assembled from 12 subunits with tetrahedral (23) symmetry (Figure 1) [31]. The subunit structure has a four-helix bundle core; a fifth helix sits in a loop connecting the B and C helices perpendicular to the four-helix bundle.

The Dps architecture contains two types of three-fold symmetry channels. One of these channels is lined with hydrophilic amino acids that can provide access for cations from bulk solution to the interior surface. The size of this channel is similar in size to the three-fold channel of Fn, which is about 0.7-0.9 nm [4, 34]. It is proposed that once metal cations are inside the protein cage, interaction with the negatively charged interior surface can occur. This interaction facilitates a similar oxidative mineralization reaction described for ferritin. The electrostatic surface of the interior of LiDps is similar to the interior surface of Fn, with clusters of glutamic acid residues that can be involved in mineral core nucleation. Utilization of Dps as a size constrained reaction template for nanoparticles synthesis is introduced below.

Reports of a Dps structure (from *Halobacterium salinarium*) in which the protein crystals were incubated with varying amounts of iron. Small clusters of Fe ions were identifiable, and several iron ions were seen bound to specific negatively charge amino acids in the protein shell. This example is the first to show a precursor to the already structurally identified mineral core[35]. The potential for using the Dps proteins to understand their role in both biomineralization and biomimetic materials synthesis has been enhanced by recent discovery and structural characterization of two Dps proteins from hyperthermophilic microorganisms, which exhibit elevated thermal stability, an ideal property for synthetic applications[7, 8].

Biomedical, Technological and Catalytic Applications of Ferritins

Biomimetic synthesis of nanoparticles; lessons from ferritins

As described above, the inherent nature of ferritin is sequestration and accumulation of iron as a form of ferrihydrite [13, 17, 23]. Mann and co-workers have demonstrated that ferromagnetic iron oxide nanoparticles can be artificially synthesized in the interior cavity of apo-ferritin (empty ferritin) cages[36-39]. The mineralized ferritin cages have iron oxide cores with homogeneous size distribution (7.3 ± 1.4 nm) that are almost indistinguishable from naturally formed iron oxide cores in holo-ferritin. This work has opened a new avenue for making nanoparticles using biomimetic processes, allowing iron oxides, as well as a

variety of inorganic nanoparticles, to be synthesized within apo-ferritin using similar methods. Using the surface directed electrostatic model as a guiding principle, ferritin has been used as a template for the synthesis of non-native minerals including Mn(O)OH and Mn_3O_4[40-42], Co(O)OH and Co_3O_4[43-45], $Cr(OH)_3$[46], $Ni(OH)_3$[46], Eu(O)OH[47], In_2O_3[48], TiO_2[47], iron phosphate and iron arsanate[49], FeS[40, 50], CdS[51], CdSe[52] and ZnSe[53]. The fact that these mineralization reactions are not specific to iron suggests that the electrostatic character of the interior surface of the protein cage plays an important role in mineralization. In the case of ZnSe, it is necessary for Zn^{2+} to be added prior to Se^{2-} in the synthetic process[53]. This has been explained by the directing electrostatic influence of the protein, which concentrates cations on the interior of the cage first, allowing for the spatially selective ZnSe particle to form inside the cage. Furthermore, metallic nanoparticles such as Pd[54, 55], Ag[56, 57], Cu[57-59], Ni[57, 60], Co[57, 60], CoPt[61] and Au/Pd bimetallic alloy[62] have been prepared via pre-incubation of the ferritin with metal salt followed by reduction of the salt using a reducing agent such as $NaBH_4$ or citrate (and light). These studies also indicate that the electrostatic interaction of cationic metal ions with the ferritin cages is key for accumulation of the ions inside of the cages, which can then be reduced to form metallic nanoparticles.

While most of the work discussed above utilized mammalian ferritins, ferritins from other organisms can have cage-like morphology and size identical to mammalian ferritins as well as unique physical and chemical properties that can be useful for material synthesis. For example, a ferritin isolated from a thermophilic archaeon, *Pyrococcus furiosus*, retains its cage-like structure even at 120°C[63], which makes the protein useful as a template for magnetite synthesis at higher temperatures than can be used with human ferritin[64]. This protein has also been used as template to demonstrate the transformation of ferrihydrite to the semiconducting hematite structure (α-Fe_2O_3) under reflux conditions in the presence of trace amounts of reducing agent with demonstrated photocatalytic activity[65].

As is described in the previous section, Dps proteins possess a cage-like structure and negatively charged interior surface similar to ferritins. Therefore, the Dps –encapsulated nanoparticles including Co(O)OH and Co_3O_4[66], γ-Fe_2O_3[67, 68], CdS[69] and Pt[70] have been synthesized using conceptually the same approach as that of ferritins. However, the resulting-nanoparticles are extremely small as Dps proteins have smaller interior cavity of 5nm than that of 8nm in ferritins. For example, it has been reported that the particle diameter of Co_3O_4 formed inside of LisDps was 4.34 ± 0.55nm[66]. Using the Dps cages as size constrained reaction templates has allowed synthetic control to obtain smaller nanoparticles than ferritins. Recent work describing a genetically redesigned Dps mutant in which interior surface was altered from hydrophilic to hydrophobic highlights versatility of the protein cage as a template and the potential for entrapment of an entirely new class of molecules/materials[71].

Biomedical application: MRI contrast agents

The inherent biological function of ferritin to store iron as ferric oxyhydroxide nanoparticles can be exploited for use in magnetic resonance imaging (MRI). Since the ferric oxyhydroxide core is superparamagnetic, ferritin can function as an endogenous T_2 enhanced MRI contrast agent[13]. This is useful as iron metabolism, and thus ferritin levels, are altered in a number of diseases. Therefore it has been proposed that endogenous ferritin can act as an MRI reporter protein, which would allow for the amount of iron in human tissues such as the liver, spleen, and brain to be assessed[72-74]. Recently, it has also been proposed that ferritin could serve as a means of monitoring transgene expression using MRI[75, 76]. However, endogenous ferritin has a 10 – 100 fold lower relaxivity per iron at clinically relevant magnetic field strengths as compared to commercially available synthetic iron oxide nanoparticles.[73, 77]. The relaxivity of mineralized ferritin can be modulated by

allowing it to aggregate in a controlled manner, and it has been demonstrated that both aggregate size and intra-aggregate perturber spacing affect the R_2 relaxivity[77, 78]. Another strategy to overcome this drawback is to utilize ferritin that has been mineralized with superparamagnetic iron oxide nanoparticles, which exhibit a much higher R_2 compared to endogenous ferritin [36, 37, 79]. In the following section, we will focus on the development of synthetic ferritin-encapsulated iron oxide nanocomposites (magnetoferritin) for use as MRI contrast agents.

It recently has been demonstrated that recombinant human HFn is a suitable platform for synthesis and encapsulation of magnetite nanoparticles. The average particle size can be controlled within a narrow size distribution ranging from 3.6nm to 5.8 nm depending upon the amount of iron loaded per cage. The R_1 and R_2 relaxivity of the mineralized HFn increases with increasing iron loading per cage (i.e. the particle size). At loading levels of 5000 iron atoms per cage the R_1 and R_2 relaxivity, as well as T2* signal loss and MR image quality of the sample, are comparable to those of commercially available small superparamagnetic iron oxide (SPIO) and ultrasmall superparamagnetic iron oxide (USPIO) contrast agents [79].

Fluorescently labeled HFn cages are accumulated significantly more in an atherosclerotic plaque lesion than in a contralateral control induced in a mouse model. Furthermore, *in vivo* MRI assessment of the atherosclerotic mouse model has demonstrated that a statistically significant decrease of the carotid artery lumen caliber size was observed 24h and 48h post-injection of the mineralized HFn, but only if the atherosclerotic plaque was present in the artery (Figure 4)[80]. The decrease of lumen size is most likely due to the T2* signal loss effect of the mineralized HFn which had accumulated in the macrophages found in the lesion. These findings suggest that ferritin that has been mineralized with magnetite could be a promising MRI contrast agent used to monitor inflammatory events induced by macrophages such as atherosclerotic plaque progression.

An alternative approach to entrap an MR imaging agent into ferritin has been proposed[81]. In this method, the ferritin protein cage was disassembled into subunits under low pH buffered conditions and subsequently reassembled into the cage structure at near neutral pH in the presence of a T_1 enhanced MRI contrast agent, GdHPDO3A. As a result, about 10 GdHPDO3A molecules per cage were entrapped within the reassembled ferritin cage. The GdHPDO3A-ferritin complex exhibited high R1 relaxivity of water protons, thereby showing its potential for applications as an MRI contrast agent.

Biomedical application: Cell Specific Targeting

Ferritin cages possess three distinct surfaces: the exterior surface, the interior surface and interface between subunits[82]. From a biomedical application viewpoint the exterior surface is an appropriate platform to display a cell specific targeting ligand[83], while the interior cavity can hold imaging or therapeutic agents. Modification of the exterior surface can be achieved either chemically or genetically. Since the high-resolution crystal structures of many of the proteins in the ferritin family have been determined, we can introduce a modification at a desired location. For instance, the amino acid sequence RGD-4C (CDCRGDCFC), known to bind integrins $\alpha_v\beta_3$ and $\alpha_v\beta_5$[84], has been genetically conjugated with N-terminal of HFn, which is exposed to the exterior[85]. The HFn mutant (RGD4C-Fn) exhibited a cage-like structure indistinguishable from the wild-type HFn by either size or morphology. Furthermore, magnetite nanoparticles were successfully prepared in the RGD4C-Fn using the same method used with HFn. These results suggest introduction of the RGD-4C peptide does not significantly disturb cage assembly and mineralization capability. Fluorescently labeled RGD4C-Fn showed specific affinity with amelanotic melanoma cells and THP-1 monocyte cells, which are known to overexpress integrin $\alpha_v\beta_3$

(Figure 5)[86]. In addition, TEM observation revealed that the mineralized RGD4C-Fn was taken up by macrophages more efficiently than the mineralized HFn alone. These findings suggest that cell/tissue specific delivery of imaging and therapeutic agents can be achieved by engineering of the exterior surface of protein cages[86].

Catalytic Applications

Protein cages similar to ferritin are expected to provide a unique environment for some catalytic reactions because the cages have an interior environment that is distinct from the exterior environment. Watanabe, Ueno and co-workers first demonstrated size-constrained synthesis of palladium (Pd^0) inside ferritin, which can catalyze hydrogenation of olefin[54]. It is worth noting that the ferritin-encapsulated Pd shows size selective catalytic activity of substrate, i.e. less catalytic activity for larger olefin molecules. This is probably because the substrates access the interior cavity of the cage through relatively small channels located between subunits. Additionally, they recently reported Au core-Pd shell bimetallic nanoparticle synthesized in ferritin exhibits a 2.5 fold higher catalytic activity than the Pd nanoparticle in ferritin[62].

Hydrogenase enzymes mimic catalysts that can produce hydrogen gas from protons have been prepared by using protein cages[70, 87]. Platinum (Pt^0) formed within the interior cavity of the protein works as an active site to reduce protons to hydrogen gas analogously to the unique biologically active metal clusters found in hydrogenase enzymes. Detailed analysis of Pt^0 nanocluster size and hydrogen production efficiency relation revealed that there is a size dependent threshold of Pt^0 cluster to produce hydrogen gas[70].

Ferritin protein cages have also been exploited as scaffold proteins to design artificial organometalloenzymes[88-90]. For example, it has been demonstrated that organometallic a Rh(nbd) (nbd = norbornadiene) complex is immobilized at specific sites of a ferritin[88]. The Rh(nbd) loaded ferritin can catalyze polymerization of phenylacetylene within the cage (Figure 6)[88]. The molecular weight distribution of the polymer prepared in the ferritin cage is narrower that that obtained by $[Ru(nbd)Cl]_2$ in the absence of ferritin. It was also reported that a Pd(allyl) complex coordinates as a dinuclear complex in ferritin through addition of $[Pd(allyl)Cl]_2$[89]. The obtained material can catalyze the Suzuki-Miyaura coupling reaction of 4-iodoaniline and phenylboronic acid to afford 4-phenyl. Substituting a Pd-coordinated His residue to an Ala residue altered the catalytic activity. Together, these results suggest that highly effective “artificial metalloenzymes” could be developed by rational design of a metal coordination site within the ferritin protein cage.

Electronic and magnetic application

Protein cages also have great potential as useful building blocks in the fabrication of electronic devices[91]. Rapid progress in circuit miniaturization achieved by sophistication of top-down approaches, such as photolithography, has allowed for doubling of chip performance every two years for the past fifty years[91]. However, the conventional methods used to fabricate electronic devices are reaching theoretical limits. The combination of a bottom-up approach with the current top-down process is expected to provide a break-through allowing for further miniaturization of electronic devices. Protein cages are ideal nano-building blocks for the fabrication of nano-device by bottom-up approach since they have excellent homogeneity in size, even at an atomic level, and the versatility to impart functionality by design. Yamashita and his co-workers have utilized ferritin and Dps-templated metal oxide nanoparticles as building units and developed what has been called the bio-nano process (BNP) for the fabrication of metal-oxide-semiconductors (MOS) such as a floating nanodot gate memory device or low-temperature polycrystalline silicon thin film transistor flash memory[91-95]. The performance and characteristics of the MOS

devices depend upon size, shape, and density of nanodot array. In a recent paper, it was demonstrated that BNP has an advantage in control of these parameters[96]. Fabrication of a two-dimensional array of protein cage-templated nanoparticles is critical in preparation of these devices. They have tested two techniques to make two-dimensional arrays of nanoparticles. One uses electrostatic interaction between the protein cages and substrate [94, 97, 98]. The exterior surface of ferritin and Dps, and the Si substrate are all negatively charged near neutral pH. Therefore, the cages can electrostatically adsorb on a designed area of a Si substrate modified to have a positively charged surface (Figure 7)[97]. The other method utilizes a specific peptide discovered by a phage display technique, which exhibits specific binding to a targeted substrate[99-102]. A titanium binding peptide (RKLPDA) or gold binding peptide (LKAHLPPSRLPS) was introduced to the exterior surface of ferritin, and it was demonstrated that the engineered ferritin can selectively adhere to titanium or gold on the substrate[100-102].

The ability to control the magnetic properties of synthesized nanoparticles is important in magnetic device applications. Protein cages, like ferritin, provide both a size and shape constrained reaction environment which allows us to tailor magnetic properties of the synthesized magnetic nanoparticles. For example, size dependent magnetic property control has been demonstrated either by changing the size of template protein cages or by changing the loading factor of a metal oxide precursor [85, 103]. More interestingly, magnetic exchange bias behavior, which is of considerable interest for technological applications such as high-density recoding and sensors, was observed if ferrimagnetic $Co_xFe_{3-x}O_4$ and antiferromagnetic Co_3O_4 nanoparticles were formed together inside of a single ferritin cage[104] (Figure 8). These findings indicate the potential of the biomimetic approach using protein cages as templates for making magnetic nanoparticles.

Nanoparticle Assembly (growth), Protein Cage Assembly and Janus-like Protein Cages

Monitoring cluster growth in Dps and Ferritin by mass spectrometry

Although the ferritin and Dps protein cages have been widely and successfully used as templates for nanomaterials syntheses, the processes of metal ion accumulation and nanoparticle formation within the protein cages are still poorly understood processes. This is mainly due to the lack of appropriate analytical tools with sufficient resolution and accuracy to detect multiple transient state species simultaneously.

Mass spectrometry (MS) has become a central part of chemistry and biological research since the inventions of electrospray ionization (ESI)[105] and matrix-assisted laser desorption ionization (MALDI)[106]. Both ESI-MS and MALD-MS essentially provide molecular mass information for large proteins in complex biological samples with high speed, accuracy and sensitivity. In biological research, mass spectrometry has mainly been used to identify unknown components of samples and detect post-translational modifications by molecular mass. Combination of ESI and time-of-flight (TOF) mass analyzer make it possible to measure the mass of large non-covalent macromolecular complexes as well as individual protein components of complexes. In addition to protein only macromolecular complexes, it has been demonstrated that interactions between protein macromolecules and metal ions or nanoclusters can be preserved, allowing metal deposition to be monitored by tracking mass increases.[68, 70] Mass spectrometry has sufficient mass accuracy and resolution to discriminate two to three metal ions depending on the atomic masses of metal ions. Therefore, it is possible to concurrently detect multiple populations distributed within an ensemble and monitor their changes individually instead of averaging over all signals.

Dps protein cages are excellent model systems to investigate the process of biomimetic nanomaterials syntheses because they have an intrinsic biomineralizing capability and robustness at high temperature, as well as a small number of subunits.[34, 66, 67] Additionally, the defined small cavity size of Dps[34] allows for the synthesis of extremely small nanomaterials[66-68, 70].

Listeria innocua Dps (LiDps) biomineralizes Fe as a nanoparticle of amorphous ferric oxyhydroxide under physiological conditions. However, treatment of the LiDps at pH 8.5 and 65 °C with 400 Fe^{2+} per cage and substoichiometric amounts of H_2O_2 (2:1, Fe:H_2O_2) results in the formation of maghemite (γ-Fe_2O_3).[67, 68] This biomimetic synthesis allows for the formation of well-defined crystalline nanoparticles with a narrow size distribution within the LiDps cages. This mineralization process within LiDps can be monitored using novel mass spectrometric methods.

Different sizes of maghemite were mineralized within LiDps by loading various amounts of Fe^{2+}. These mineralized samples were then subjected to mass spectrometric analyses (Figure 9). ESI generally produces a series of multiply charged ions and the charges (z) are generally distributed as a continuous series with a Gaussian intensity distribution (… z−2, z −1, z, z+1, z+2…).

If there are multiple species in a mass spectrum, multiple Gaussian charge distributions can be detected and the molecular masses of each species can be determined from the charges and the observed mass-to-charge (m/z) ratio values.

Charge state distributions of Fe mineralized LiDps shifted to higher m/z according to the increase of initial Fe^{2+} ion loadings representing particle growth (Figure 9). Mass spectra of Fe mineralized LiDps exhibited the presence of more than one mass distribution and high mass resolution make it possible to determine exact amounts of Fe mineralized at each step (Figure 9). This capability of detecting multiple species simultaneously also allowed for the detection of long-lived Fe accumulating intermediate (12 Fe bound LiDps) state in all samples as well as individual species within the ensemble population. By comparison with a ferroxidase center knock-out mutant of LiDps, which lacks Fe binding and mineralization, it was confirmed that this early 12 Fe accumulating stage is indeed necessary for successful maghemite nanoparticle formation within protein cages[68]. A two-stage growth process model was established based on mass spectrometric data and verified with a simple kinetic model.

Pt^0 nanoparticles are known to be excellent catalysts for proton reduction and hydrogen production.[70, 87, 107] To elucidate the relationship between platinum (Pt) nanocluster sizes and catalytic activity of hydrogen production, similar mass spectrometric approaches were performed. For the controlled synthesis of Pt nanoclusters, the interior surface of LiDps was modified both genetically and chemically to have metal binding ligands (phenanthroline). Pt^{2+} ion binding to LiDps and the Pt^0 nanocluster growth within modified LiDps (phen-LiDps) were independently monitored by mass spectrometry[70]. Charge state distributions of both Pt^{2+} ion bound (black) and Pt^0 nanoclustered phen-LiDps (red) were shifted to higher m/z in accordance with the increasing numbers of Pt^{2+} ions loaded with different degrees (Figure 10). Only one population was observed at each Pt^{2+} ion loading (Figure 10) implying that binding or nanocluster formation events occur homogeneously throughout the cage population rather than in an all-or-nothing manner. Mass analyses demonstrate that the introduced Pt^{2+} ions first enter the cages and bind to the covalently attached phenanthroline moeity and that free Pt^{2+} ions inside are recruited by the pre-bound Pt^{2+} ions upon photoreduction to form the Pt^0 nanoclusters. These approaches allowed the transition from metal binding to nucleation and nanocluster formation to be followed

precisely. The hydrogen production catalytic activity of Pt mineralized LiDps was determined and correlated with nanocluster sizes. While the phen-LiDps samples with equal to or less than 45 Pt^0 produced hydrogen near baseline levels, the 75 Pt^0 containing phen-LiDps generated approximately four times more hydrogen than the background level[70]. These data suggested that 75 Pt atoms form a sufficiently large nanocluster for hydrogen production compared to the multiple nanoclusters within phen-LiDps. In contrast, the cages containing 45 Pt or lower Pt atoms appear to have failed to form a sufficiently large cluster to catalyze hydrogen production.

Chimeric assembly of protein cages from differently modified subunits

Many cellular activities are achieved by the formation of non-covalent macromolecular complexes. Association/dissociation reactions are intimately involved in recognition phenomena, such as enzyme-substrate interaction and assembly of oligomeric proteins, and these processes are tightly controlled by precise recognition and conformational adaptation upon contact. One of the most fundamental but challenging subjects of protein engineering is to understand the protein-protein interactions in macromolecular complexes and manipulate these systems at the molecular level.

Ferritin is a naturally chimeric protein cage, which regulates its iron forming activity through different hetero-forms. In mammalian cells, ferritin is composed of two iso-forms of subunits, H and L, with ratios varying from species to species and from tissue to tissue. The subunits, H and L, have complementary functions in iron oxide formations. While the H chain has a ferroxidase center where oxidation of iron is initiated, the L chain has acidic residues where nucleation and growth of iron oxide cores occurs. The activity of ferritin relies on the ratio of H and L chains and each species or tissue has its own hetero-forms to adjust to its unique needs.[13]

A mimic of the precisely controlled macromolecular self-assembly has been attempted through genetic and chemical modifications.[108, 109] However, it is still challenging to manipulate subunit self-assembly in a controlled way and to analyze assembled products precisely at the molecular level.[110]

By combining genetic and chemical modifications, bifunctional Dps chimeric cages having metal binding ligands (phenanthroline) inside and fluorophores (flouresceine) outside were constructed in a controlled manner similar to the mammalian ferritin chimera.[110] Two different functional groups were individually attached to either the inside (phen-LiDps) or outside (F5M-LiDps) of the cage. Each internally and externally functionalized LiDps protein cage was dissociated into subunits by lowering the pH (Figure 11).[110] Analytical ultra-centrifugation and mass spectrometry data revealed that both dissociated phen- and F5M-LiDps subunits exist predominantly as monomers in solution at pH 2.0. Bifunctional chimeric LiDps protein cages were constructed by mixing individually modified and dissociated subunits in various desired ratios and reassembled by slowly raising the pH to 7 (Figure 11). Mass spectrometric analyses of reassembled cages demonstrated that an increased ratio of F5M subunits, the heavier subunit, resulted in shifts of charge state distribution to higher *m/z* (Figure 11) clearly demonstrating mixed incorporation of both phen and F5M LiDps subunits into a reassembled cage. A binomial distribution model[111] fitting the experimental mass spectra revealed that the formation of chimeric cages can be well described by a simple binomial distribution in which the assembly unit is a monomer that obeys the initial mixing ratios instead of forming two individual cage populations (Figure 11).

Ferritin and Dps protein cages have a similar monomeric fold, four helix bundle structure, and a helix swapping between bacterioferritin (BFR) and Dps from *E. coli* has been

attempted to control nanoarchitectures of the protein cages.[109] While many of the helix swapped BFR do not self-assemble, those of Dps form larger protein cages containing the same 12 subunits.[109]

Preparation of Janus like protein cages

Protein cages have been widely used as nanoscale building blocks for fabricating higher order nanostructures, such as ordered planar arrays,[112-114] nanowires,[115, 116] nanoelectronic devices,[94, 117, 118] and layer-by-layer (LbL) assemblies,[119-125] either by using the endogenous self-assembly properties of the proteins[113] or by modifying the surfaces of the cages to accomplish directed assembly.[119-125] Genetic and chemical modification of the exterior surface of protein cage architectures allows site specific attachment and presentation of various types of molecules including affinity tags, antibodies, fluorophores, carbohydrates, nucleic acids, and targeting peptides.[85, 108, 110, 126-134] Multi-ligand presentation on a single protein cage surface has been achieved by labeling with two different reagents either simultaneously or sequentially[85, 126-134] or by assembly of pre-functionalized subunits in controlled ratios[108, 110]. While the highly symmetric nature of protein cages is advantageous for the formation of isotropic hierarchal structures, it is necessary to break the functional symmetry of the cage to achieve topological control for applications such as directed molecular recognition, controlled anisotropic hierarchal assembly, and polarized multi-component presentation.[135-137] However, symmetry of protein cages presents a formidable challenge in controlling the spatial location of functional groups to achieve toposelectivity.

To generate Janus-like protein cages, which are cages with dual architectures and purposes, the exterior surfaces of LiDps cages were toposelectively modified with two different functionalities, the fluorophore - fluorescein and the affinity tag – biotin, using a masking/unmasking method on solid supports (Figure 12).[138] One side of the symmetric LiDps was protected from labeling through binding to a solid support and exposed side was modified with maleimide-PEG_2-biotin (MPB) on solid beads (Figure 12). Subsequently, the MPB-reacted LiDps cages were eluted from the beads by reduction and the free cysteine residues on subunits, which were previously masked by disulfide formation with the beads, were labeled with fluorescein-5-maleimide (F5M) in solution (Figure 12). The extent of modifications at each step was evaluated by measuring subunit and whole cage masses. The degree of distributions of the two functionalities could be controlled using different solid supporting materials. Their localized distributions were confirmed by controlled layer-by-layer (LbL) formation using realtime quartz-crystal microbalance (QCM) measurement and atomic force microscopy (AFM)[138]. Spatially controlled surface presentation of multiple functional groups on a protein cage enables the cages to be used as polarized nanoscale building blocks for directed hierarchal assembly, as well as for fabricating nanoscale cargoes with distinct functional groups on each hemisphere.

With respect to biomedical applications of engineered systems, toposelective modification of multifunctional nanoplatforms promises realization of sophisticated designs for targeting cells with drugs and imaging agents. Janus-like protein cages were used as new types of targeting nanoplatforms by docking the universal coupling protein, streptavidin (StAv).[137] Modular asymmetric functionalization with an antibody provides a method to easily adapt a multifunctional nanoplatform for targeting a diverse set of cell epitopes and the targeting and detecting capability of the microbial pathogen, *Staphylococcus aureus*, were demonstrated by coupling with biotinylated monoclonal antibody (mAb) against *S. aureus*. [137] The asymmetrical positioning of the StAv coupling protein provides an opportunity for realizing imaging or drug delivery strategies that rely on a polarized orientation of targeted functional groups with respect to the cell surface.

Summary

In conclusion, the ferritin superfamily of proteins has proved to be a rich and productive set of biomolecular templates for directed materials synthesis. This has included both the nucleation and growth of inorganic nanoparticles as well as the chemical and genetic manipulation of the protein to yield materials with applications from medicine to electronics.

References Cited

1. Koeck PJB, Kagawa HK, Ellis MJ, Hebert H, Trent JD. Two-dimensional crystals of reconstituted .beta.-subunits of the chaperonin TF55 from Sulfolobus shibatae. Biochim Biophys Acta. 1998; 1429:40–44. [PubMed: 9920382]
2. Trent JD. A review of acquired thermotolerance, heat-shock proteins, and molecular chaperones in archaea. FEMS Microbiol Rev. 1996; 18:249–258.
3. Kim KK, Kim R, Kim SH. Crystal structure of a small heat-shock protein. Nature. 1998; 394:595–599. [PubMed: 9707123]
4. Bozzi M, Mignogna G, Stefanini S, Barra D, Longhi C, Valenti P, Chiancone E. A Novel Non-heme Iron-binding Ferritin Related to the DNA-binding Proteins of the Dps Family in *Listeria innocua*. J Biol Chem. 1997; 272:3259–3265. [PubMed: 9013563]
5. Grant RA, Filman DJ, Finkel SE, Kolter R, Hogle JM. The crystal structure of Dps, a ferritin homolog that binds and protects DNA. Nature Structural Biology. 1998; 5:294–303.
6. Grove A, Wilkinson SP. Differential DNA binding and protection by dimeric and dodecameric forms of the ferritin homolog Dps from Deinococcus radiodurans. J Mol Biol. 2005; 347:495–508. [PubMed: 15755446]
7. Ramsay R, Wiedenheft B, Allen M, Gauss GH, Lawrence CM, Young M, Douglas T. Dps-like protein from the hyperthermophilic archaeon *Pyrococcus furiosus*. J Inorg Biochem. 2006; 100:1061–1068. [PubMed: 16412514]
8. Wiedenheft B, Mosolf J, Willits D, Yeager M, Dryden KA, Young M, Douglas T. An archaeal antioxidant: Characterization of a Dps-like protein from Sulfolobus solfataricus. Proceedings of the National Academy of Sciences of the United States of America. 2005; 102:10551–10556. [PubMed: 16024730]
9. Zhao G, Ceci P, Ilari A, Giangiacomo L, Laue TM, Chiancone E, Chasteen ND. Iron and Hydrogen Peroxide Detoxification Properties of Dps. A Ferritin-Like DNA Binding Protein of *Escherichia coli*. J Biol Chem. 2002 epub.
10. Bancroft JB, Bracker CE, Wagner GW. Structures derived from cowpea chlorotic mottle and brome mosaic virus protein. Virology. 1969; 38:324–335. [PubMed: 5784855]
11. Crick FH, Watson JD. Structure of small viruses. Nature. 1956; 177:473–475. [PubMed: 13309339]
12. Douglas T, Strable E, Willits D, Aitouchen A, Libera M, Young M. Protein engineering of a viral cage for constrained nanomaterials synthesis. Advanced Materials. 2002; 14:415–418.
13. Harrison PM, Arosio P. Ferritins: Molecular properties, iron storage function and cellular regulation. Biochimica Et Biophysica Acta-Bioenergetics. 1996; 1275:161–203.
14. Matias PM, Tatur J, Carrondo MA, Hagen WR. Crystallization and preliminary X-ray characterization of a ferritin from the hyperthermophilic archaeon and anaerobe Pyrococcus furiosus. Acta Crystallogr F-Struct Biol Cryst Commun. 2005; 61:503–506.
15. Hempstead PD, Yewdall SJ, Fernie AR, Lawson DM, Artymiuk PJ, Rice DW, Ford GC, Harrison PM. Comparison of the three-dimensional structures of recombinant human H and horse L ferritins at high resolution. J Mol Biol. 1997; 268:424–448. [PubMed: 9159481]
16. Kurtz DM Jr. Structural similarity and functional diversity in diiron-oxo proteins, JBIC. J Biol Inorg Chem. 1997; 2:159–167.
17. Lawson DM, Artymiuk PJ, Yewdall SJ, Smith JMA, Livingstone JC, Treffry A, Luzzago A, Levi S, Arosio P, Cesareni G, Thomas CD, Shaw WV, Harrison PM. Solving the Structure of Human H-Ferritin by Genetically Engineering Intermolecular Crystal Contacts. Nature. 1991; 349:541–544. [PubMed: 1992356]

18. Mayer DE, Rohrer JS, Schoeller DA, Harris DC. Fate of Oxygen during Ferritin Iron Incorporation. Biochemistry. 1983; 22:876–880. [PubMed: 6838829]
19. Cornell, R.; Schwertmann, U. The Iron Oxides. 2. Wiley-VCH; Weinheim: 2003.
20. Michel FM, Ehm L, Antao SM, Lee PL, Chupas PJ, Liu G, Strongin DR, Schoonen MA, Phillips BL, Parise JB. The structure of ferrihydrite, a nanocrystalline material. Science. 2007; 316:1726–1729. [PubMed: 17525301]
21. Douglas T, Ripoll DR. Calculated electrostatic gradients in recombinant human H-chain ferritin. Protein Sci. 1998; 7:1083–1091. [PubMed: 9605313]
22. Theil EC, Takagi H, Small GW, He L, Tipton AR, Danger D. The Ferritin Iron Entry and Exit Problem. Inorg Chim Acta. 2000; 297:242–251.
23. Chasteen ND, Harrison PM. Mineralization in ferritin: An efficient means of iron storage. Journal of Structural Biology. 1999; 126:182–194. [PubMed: 10441528]
24. Juan SH, Aust SD. The Effect of Putative Nucleation Sites on the Loading and Stability of Iron in Ferritin. Arch Biochem Biophys. 1998; 350:259–265. [PubMed: 9473300]
25. Santambrogio P, Levi S, Cozzi A, Corsi B, Arosio P. Evidence that the specificity of iron incorporation into homopolymers of human ferritin L- and H-chains is conferred by the nucleation and ferroxidase centres. Journal of Biological CHemistr. 1996; 314:139–144.
26. Atkins, P. Physical Chemistry. 6. W.H. Freeman and Company/Oxford English Press; New York: 1998.
27. Kinraide TB, Yermiyahu U, Rytwo G. Computation of Surface Electrical Potentials of Platn Cell Membranes. Plant Physiol. 1998; 118:505–512. [PubMed: 9765535]
28. Bard, AJ.; Faulkner, LR. Electrochemical Methods Fundamentals and Applications. John Wiley and Sons; New York: 1980.
29. Almiron M, Link AJ, Furlong D, Kolter R. A novel DNA-binding protein with regulatory and protective roles in starved *Escherichia coli*. Genes Dev. 1992; 6:2646–2654. [PubMed: 1340475]
30. Ceci P, Ilari A, Falvo E, Chiancone E. The Dps protein of Agrobacterium tumefaciens does not bind to DNA but protects it toward oxidative cleavage. Journal of Biological Chemistry. 2003; 278:20319–20326. [PubMed: 12660233]
31. Ilari A, Savino C, Stefanini S, Chiancone E, Tsernoglou D. Crystallization and preliminary X-ray crystallographic analysis of the unusual ferritin from Listeria innocua. Acta Crystallogr Sect D-Biol Crystallogr. 1999; 55:552–553. [PubMed: 10089376]
32. Marjorette M, Pena O, Bullerjahn GS. The DpsA Protein of *Synechococcus* sp. Strain PCC7942 Is a DNA-binding Hemoprotein. The Journal of Biological Chemistry. 1995; 270:22478–22482. [PubMed: 7673237]
33. Reindel S, Schmidt CL, Anemuller S, Matzanke BF. Characterization of a non-haem ferritin of the Archaeon Halobacterium salinarum, homologous to Dps (starvation-induced DNA-binding protein). Biochem Soc Trans. 2002; 30:713–715. [PubMed: 12196173]
34. Ilari A, Stefanini S, Chiancone E, Tsernoglou D. The dodecameric ferritin from Listeria innocua contains a novel intersubunit iron-binding site. Nature Structural Biology. 2000; 7:38–43.
35. Zeth K, Offermann S, Essen LO, Oesterhelt D. Iron-oxo clusters biomineralizing on protein surfaces: structural analysis of Halobacterium salinarum DpsA in its low- and high-iron states. Proc Natl Acad Sci U S A. 2004; 101:13780–13785. [PubMed: 15365182]
36. Meldrum FC, Heywood BR, Mann S. Magnetoferritin: in vitro synthesis of a novel magnetic protein. Science. 1992; 257:522–523. [PubMed: 1636086]
37. Bulte JWM, Douglas T, Mann S, Frankel RB, Moskowitz BM, Brooks RA, Baumgarner CD, Vymazal J, Strub MP, Frank JA. Magnetoferritin - Characterization of a Novel Superparamagnetic Mr Contrast Agent. Jmri-Journal of Magnetic Resonance Imaging. 1994; 4:497–505.
38. Mann S, Archibald DD, Didymus JM, Douglas T, Heywood BR, Meldrum FC, Reeves NJ. Crystallization at inorganic-organic interfaces: biominerals and biomimetic synthesis. Science. 1993; 261:1286–1292. [PubMed: 17731856]
39. Wong KKW, Douglas T, Gider S, Awschalom DD, Mann S. Biomimetic snthesis and characterization of magnetic proteins (magnetoferritin). Chem Mater. 1998; 10:279–285.

40. Mann S, Meldrum FC. Controlled Synthesis of Inorganic Materials Using Supramolecular Assemblies. Advanced Materials. 1991; 3:316–318.
41. Mackle P, Charnock JM, Garner CD, Meldrum FC, Mann S. Characterization of the Manganese Core of Reconstituted Ferritin by X-Ray-Absorption Spectroscopy. Journal of theAmerican Chemical Society. 1993; 115:8471–8472.
42. Meldrum FC, Douglas T, Levi S, Arosio P, Mann S. Reconstitution of Manganese Oxide Cores in Horse Spleen and Recombinant Ferritins. J Inorg Biochem. 1995; 58:59–68. [PubMed: 7738539]
43. Douglas T, Stark VT. Nanophase Cobalt Oxyhydroxide Mineral Synthesized within the Protein Cage of Ferritin. Inorg Chem. 2000; 39:1828–1830. [PubMed: 12526579]
44. Tsukamoto R, Iwahor K, Muraoka M, Yamashita I. Synthesis of Co3O4 nanoparticles using the cage-shaped protein, apoferritin. Bulletin of the Chemical Society of Japan. 2005; 78:2075–2081.
45. Tsukamoto R, Muraoka M, Fukushige Y, Nakagawa H, Kawaguchi T, Nakatsuji Y, Yamashita I. Improvement Of Co3O4 Nanoparticle Synthesis in Apoferritin Cavity by Outer Surface PEGylation. Bulletin of the Chemical Society of Japan. 2008; 81:1669–1674.
46. Okuda M, Iwahori K, Yamashita I, Yoshimura H. Fabrication of nickel and chromium nanoparticles using the protein cage of apoferritin. Biotechnology and Bioengineering. 2003; 84:187–194. [PubMed: 12966575]
47. Klem MT, Mosolf J, Young M, Douglas T. Photochemical Mineralization of Europium, Titanium, and Iron Oxyhydroxide Nanoparticles in the Ferritin Protein Cage. Inorg Chem. 2008
48. Okuda M, Kobayashi Y, Suzuki K, Sonoda K, Kondoh T, Wagawa A, Kondo A, Yoshimura H. Self-organized inorganic nanoparticle arrays on protein lattices. Nano Letters. 2005; 5:991–993. [PubMed: 15884908]
49. Polanams J, Ray AD, Watt RK. Nanophase Iron Phosphate, Iron Arsenate, Iron Vanadate, and Iron Molybdate Minerals Synthesized within the Protein Cage of Ferritin. Inorg Chem. 2005; 44:3203–3209. [PubMed: 15847428]
50. Douglas T, Dickson DPE, Betteridge S, Charnock J, Garner CD, Mann S. Synthesis and Structure of an Iron(Iii) Sulfide-Ferritin Bioinorganic Nanocomposite. Science. 1995; 269:54–57. [PubMed: 17787702]
51. Wong KKW, Mann S. Biomimetic synthesis of cadmium sulfide-ferritin nanocomposites. Advanced Materials. 1996; 8:928–932.
52. Yamashita I, Hayashi J, Hara M. Bio-template synthesis of uniform CdSe nanoparticles using cage-shaped protein, apoferritin. Chemistry Letters. 2004; 33:1158–1159.
53. Iwahori K, Yoshizawa K, Muraoka M, Yamashita I. Fabrication of ZnSe Nanoparticles in the Apoferritin Cavity by Designing a Slow Chemical Reaction System. Inorg Chem. 2005; 44:6393–6400. [PubMed: 16124819]
54. Ueno T, Suzuki M, Goto T, Matsumoto T, Nagayama K, Watanabe Y. Size-selective olefin hydrogenation by a Pd nanocluster provided in an apo-ferritin cage. Angew Chem Int Ed. 2004; 43:2527–2530.
55. Clemente-Leon M, Coronado E, Soriano-Portillo A, Galvez N, Dominguez-Vera JM. Permanent magnetism in apoferritin-encapsulated Pd nanoparticles. Journal of Materials Chemistry. 2007; 17:49–51.
56. Kramer RM, Li C, Carter DC, Stone MO, Naik RR. Engineered protein cages for nanomaterial synthesis. Journal of the American Chemical Society. 2004; 126:13282–13286. [PubMed: 15479082]
57. Galvez N, Fernandez B, Valero E, Sanchez P, Cuesta R, Dominguez-Vera JM. Apoferritin as a nanoreactor for preparing metallic nanoparticles. Comptes Rendus Chimie. 2008; 11:1207–1212.
58. Ceolin M, Galvez N, Dominguez-Vera JM. Thermal induced phase transitions and structural relaxation in apoferritin encapsulated copper nanoparticles. Phys Chem Chem Phys. 2008; 10:4327–4332. [PubMed: 18633553]
59. Ensign D, Young M, Douglas T. Photocatalytic synthesis of copper colloids from Cu(II) by the ferrihydrite core of ferritin. Inorganic Chemistry. 2004; 43:3441–3446. [PubMed: 15154806]
60. Galvez N, Sanchez P, Dominguez-Vera JM, Soriano-Portillo A, Clemente-Leon M, Coronado E. Apoferritin-encapsulated Ni and Co superparamagnetic nanoparticles. Journal of Materials Chemistry. 2006; 16:2757–2761.

61. Warne B, Kasyutich O, Mayes E, Wiggins JAL, Wong KKW. Self assembled nanoparticulate Co: Pt for data storage applications. Ieee Transactions on Magnetics. 2000; 36:3009–3011.
62. Suzuki M, Abe M, Ueno T, Abe S, Goto T, Toda Y, Akita T, Yamadae Y, Watanabe Y. Preparation and catalytic reaction of Au/Pd bimetallic nanoparticles in Apo-ferritin. Chemical Communications. 2009:4871–4873. [PubMed: 19652809]
63. Tatur J, Hagedoorn PL, Overeijnder ML, Hagen WR. A highly thermostable ferritin from the hyperthermophilic archaeal anaerobe Pyrococcus furiosus. Extremophiles. 2006; 10:139–148. [PubMed: 16341820]
64. Parker MJ, Allen MA, Ramsay B, Klem MT, Young M, Douglas T. Expanding the Temperature Range of Biomimetic Synthesis Using a Ferritin from the Hyperthermophile Pyrococcus furiosus. Chem Mater. 2008; 20:1541–1547.
65. Klem MT, Young M, Douglas T. Biomimetic synthesis of photoactive α-Fe2O3 templated by the hyperthermophilic ferritin from Pyrococus furiosus. J Mater Chem. in press.
66. Allen M, Willits D, Young M, Douglas T. Constrained synthesis of cobalt oxide nanomaterials in the 12-subunit protein cage from Listeria innocua. Inorganic Chemistry. 2003; 42:6300–6305. [PubMed: 14514305]
67. Allen M, Willits D, Mosolf J, Young M, Douglas T. Protein cage constrained synthesis of ferrimagnetic iron oxide nanoparticles. Advanced Materials. 2002; 14:1562–1565.
68. Kang S, Jolley C, Liepold L, Young M, Douglas T. Metal Binding to Nanoparticle Formation; Monitoring Biomimetic Iron Oxide Synthesis within Protein Cages using Mass Spectrometry. Angew Chem Int Ed. 2009
69. Iwahori K, Yamashita I. Size-controlled one-pot synthesis of fluorescent cadmium sulfide semiconductor nanoparticles in an apoferritin cavity. Nanotechnology. 2008; 19
70. Kang S, Lucon J, Varpness Z, Liepold L, Uchida M, Willits D, Young M, Douglas T. Monitoring Biomimetic Platinum Nanocluster Formation Using Mass Spectrometry and Cluster-Dependent H_2 Production13. Angew Chem Int Ed. 2008; 47:7845–7848.
71. Swift J, Wehbi WA, Kelly BD, Stowell XF, Saven JG, Dmochowski IJ. Design of functional ferritin-like protein with hydrophobic cavities. Journal of the American Chemical Society. 2006 in press.
72. Stark DD, Bass NM, Moss AA, Bacon BR, McKerrow JH, Cann CE, Brito A, Goldberg HI. Nuclear magnetic resonance imaging of experimentally induced liver disease. Radiology. 1983; 148:743–751. [PubMed: 6192464]
73. Gossuin Y, Muller R, Gillis P, Bartel L. Relaxivities of human liver and spleen ferritin. Magnetic Resonance Imaging. 2005; 23:1001–1004. [PubMed: 16376184]
74. Vymazal J, Righini A, Brooks RA, Canesi M, Mariani C, Leonardi M, Pezzoli G. T1 and T2 in the brain of healthy subjects, patients with Parkinson disease, and patients with multiple system atrophy: relation to iron content. Radiology. 1999; 211:489–495. [PubMed: 10228533]
75. Genove G, Demarco U, Xu H, Goins W, Ahrens E. A new transgene reporter for in vivo magnetic resonance imaging. Nat Med. 2005; 11:450–454. [PubMed: 15778721]
76. Cohen B, Dafni H, Meir G, Harmelin A, Neeman M. Ferritin as an endogenous MRI reporter for noninvasive imaging of gene expression in C6 glioma tumors. Neoplasia. 2005; 7:109–117. [PubMed: 15802016]
77. Bennett KM, Shapiro EM, Sotak CH, Koretsky AP. Controlled aggregation of ferritin to modulate MRI relaxivity. Biophys J. 2008; 95:342–351. [PubMed: 18326661]
78. Wood JC, Fassler JD, Meade T. Mimicking liver iron overload using liposomal ferritin preparations. Magn Reson Med. 2004; 51:607–611. [PubMed: 15004804]
79. Uchida M, Terashima M, Cunningham CH, Suzuki Y, Willits DA, Willis AF, Yang PC, Tsao PS, McConnell MV, Young MJ, Douglas T. A human ferritin iron oxide nano-composite magnetic resonance contrast agent. Magn Reson Med. 2008; 60:1073–1081. [PubMed: 18956458]
80. Terashima M, Uchida M, Kosuge H, Cunningham CH, Tsao P, Young M, Conolly SM, Douglas T, McConnell MV. Human ferritin protein cage nanoparticles as macrophage-targeted contrast agents for detecting inflammation in atherosclerosis. in preparation.

81. Aime S, Frullano L, Crich SG. Compartmentalization of a gadolinium complex in the apoferritin cavity: A route to obtain high relaxivity contrast agents for magnetic resonance imaging. Angew Chem Int Ed. 2002; 41:1017–1019.
82. Douglas T, Young M. Viruses: Making friends with old foes. Science. 2006; 312:873–875. [PubMed: 16690856]
83. Flenniken ML, Willits DA, Harmsen AL, Liepold LO, Harmsen AG, Young MJ, Douglas T. Melanoma and lymphocyte cell-specific targeting incorporated into a heat shock protein cage architecture. Chemistry & Biology. 2006; 13:161–170. [PubMed: 16492564]
84. Arap W, Pasqualini R, Ruoslahti E. Cancer treatment by targeted drug delivery to tumor vasculature in a mouse model. Science. 1998; 279:377–380. [PubMed: 9430587]
85. Uchida M, Flenniken ML, Allen M, Willits DA, Crowley BE, Brumfield S, Willis AF, Jackiw L, Jutila M, Young MJ, Douglas T. Targeting of cancer cells with ferrimagnetic ferritin cagenanoparticles. Journal of the American Chemical Society. 2006; 128:16626–16633. [PubMed: 17177411]
86. Uchida M, Willits AD, Muller K, Willis AF, Jackiw L, Jutila M, Young M, Porter AE, Douglas T. Intracellular distribution of macrophage targeting ferriti-iron oxide nanocomposite. Advanced Materials. 2009; 21:458–462.
87. Varpness Z, Peters JW, Young M, Douglas T. Biomimetic synthesis of a H-2 catalyst using a protein cage architecture. Nano Letters. 2005; 5:2306–2309. [PubMed: 16277473]
88. Abe S, Hirata K, Ueno T, Morino K, Shimizu N, Yamamoto M, Takata M, Yashima E, Watanabe Y. Polymerization of Phenylacetylene by Rhodium Complexes within a Discrete Space of apo-Ferritin. J Am Chem Soc. 2009; 131:6958–6960. [PubMed: 19453195]
89. Abe S, Niemeyer J, Abe M, Takezawa Y, Ueno T, Hikage T, Erker G, Watanabe Y. Control of the Coordination Structure of Organometallic Palladium Complexes in an apo-Ferritin Cage. Journal of the American Chemical Society. 2008; 130:10512–10514. [PubMed: 18636721]
90. Niemeyer J, Abe S, Hikage T, Ueno T, Erker G, Watanabe Y. Noncovalent insertion of ferrocenes into the protein shell of apo-ferritin. Chemical Communications. 2008:6519–6521. [PubMed: 19057765]
91. Yamashita I. Biosupramolecules for nano-devices: biomineralization of nanoparticles and their applications. Journal of Materials Chemistry. 2008; 18:3813–3820.
92. Matsui T, Matsukawa N, Iwahori K, Sano KI, Shiba K, Yamashita I. Direct production of a two-dimensional ordered array of ferritin-nanoparticles on a silicon substrate. Jpn J Appl Phys 2. 2007; 46:L713–L715.
93. Ichikawa K, Uraoka Y, Punchaipetch P, Yano H, Hatayama T, Fuyuki T, Yamashita I. Low-temperature polycrystalline silicon thin film transistor flash memory with ferritin. Jpn J Appl Phys Part 2 - Lett Express Lett. 2007; 46:L804–L806.
94. Miura A, Hikono T, Matsumura T, Yano H, Hatayama T, Uraoka Y, Fuyuki T, Yoshii S, Yamashita I. Floating nanodot gate memory devices based on biomineralized inorganic nanodot array as a storage node. Jpn J Appl Phys. 2006; 45:L1–L3.
95. Hikono T, Matsumura T, Miura A, Uraoka Y, Fuyuki T, Takeguchi M, Yoshii S, Yamashita I. Electron confinement in a metal nanodot monolayer embedded in silicon dioxide produced using ferritin protein. Appl Phys Lett. 2006; 88
96. Yamada K, Yoshii S, Kumagai S, Miura A, Uraoka Y, Fuyuki T, Yamashita I. Effects of dot density and dot size on charge injection characteristics in nanodot array produced by protein supramolecules. Jpn J Appl Phys 1. 2007; 46:7549–7553.
97. Kumagai S, Yoshii S, Yamada K, Matsukawa N, Fujiwara I, Iwahori K, Yamashita I. Electrostatic placement of single ferritin molecules. Appl Phys Lett. 2006; 88
98. Yamada K, Yoshii S, Kumagai S, Miura A, Uraoka Y, Fuyuki T, Yamashita I. Floating gate metal-oxide-semiconductor capacitor employing array of high-density nanodots produced by protein supramolecule. Jpn J Appl Phys 1. 2006; 45:8946–8951.
99. Matsui T, Matsukawa N, Iwahori K, Sano K, Shiba K, Yamashita I. Realizing a two-dimensional ordered array of ferritin molecules directly on a solid surface utilizing carbonaceous material affinity peptides. Langmuir. 2007; 23:1615–1618. [PubMed: 17279636]

100. Hayashi T, Sano K, Shiba K, Kumashiro Y, Iwahori K, Yamashita I, Hara M. Mechanism underlying specificity of proteins targeting inorganic materials. Nano Lett. 2006; 6:515–519. [PubMed: 16522054]
101. Ishikawa K, Yamada K, Kumagai S, Sano KI, Shiba K, Yamashita I, Kobayashi M. Adsorption properties of a gold-binding peptide assessed by its attachment to a recombinant apoferritin molecule. Appl Phys Express. 2008; 1
102. Sano K, Yoshii S, Yamashita I, Shiba K. In aqua structuralization of a three-dimensional configuration using biomolecules. Nano Lett. 2007; 7:3200–3202. [PubMed: 17824660]
103. Gilmore K, Idzerda YU, Klem MT, Allen M, Douglas T, Young M. Surface contribution to the anisotropy energy of spherical magnetite particles. Journal of Applied Physics. 2005; 97
104. Klem MT, Resnick DA, Gilmore K, Young M, Idzerda YU, Douglas T. Synthetic control over magnetic moment and exchange bias in all-oxide materials encapsulated within a spherical protein cage. Journal of the American Chemical Society. 2007; 129:197–201. [PubMed: 17199299]
105. Fenn JB, Mann M, Meng CK, Wong SF, Whitehouse CM. Electrospray ionization for mass spectrometry of large biomolecules. Science. 1989; 246:64–71. [PubMed: 2675315]
106. Tanaka K, Waki H, Ido Y, Akita S, Yoshida Y, Yoshida T, Matsuo T. Protein and polymer analyses up to m/z 100 000 by laser ionization time-of-flight mass spectrometry. Rapid Communications in Mass Spectrometry. 1988; 2:151–153.
107. Gratzel M. Artificial Photosynthesis - Water Cleavage into Hydrogen and Oxygen by Visible-Light. Accounts of Chemical Research. 1981; 14:376–384.
108. Gillitzer E, Suci P, Young M, Douglas T. Controlled ligand display on a symmetrical protein-cage architecture through mixed assembly. Small. 2006; 2:962–966. [PubMed: 17193150]
109. Fan RL, Boyle AL, Cheong VV, Ng SL, Orner BP, Helix A. Swapping Study of Two Protein Cages. Biochemistry. 2009; 48:5623–5630. [PubMed: 19405543]
110. Kang S, Oltrogge LM, Broomell CC, Liepold LO, Prevelige PE, Young M, Douglas T. Controlled Assembly of Bifunctional Chimeric Protein Cages and Composition Analysis Using Noncovalent Mass Spectrometry. Journal of the American Chemical Society. 2008; 130:16527–16529. [PubMed: 19554690]
111. Painter AJ, Jaya N, Basha E, Vierling E, Robinson CV, Benesch JLP. Real-time monitoring of protein complexes reveals their quaternary organization and dynamics. Chemistry & Biology. 2008; 15:246–253. [PubMed: 18355724]
112. Cheung CL, Camarero JA, Woods BW, Lin T, Johnson JE, De Yoreo JJ. Fabrication of Assembled Virus Nanostructures on Templates of Chemoselective Linkers Formed by Scanning Probe Nanolithography. Journal of the American Chemical Society. 2003; 125:6848–6849. [PubMed: 12783520]
113. McMillan RA, Howard J, Zaluzec NJ, Kagawa HK, Mogul R, Li YF, Paavola CD, Trent JD. A Self-Assembling Protein Template for Constrained Synthesis and Patterning of Nanoparticle Arrays. Journal of the American Chemical Society. 2005; 127:2800–2801. [PubMed: 15740085]
114. Nam KT, Wartena R, Yoo PJ, Liau FW, Lee YJ, Chiang YM, Hammond PT, Belcher AM. Stamped microbattery electrodes based on self-assembled M13 viruses. Proceedings of the National Academy of Sciences of the United States of America. 2008; 105:17227–17231. [PubMed: 18753629]
115. Huang Y, Chiang CY, Lee SK, Gao Y, Hu EL, Yoreo JD, Belcher AM. Programmable Assembly of Nanoarchitectures Using Genetically Engineered Viruses. Nano Letters. 2005; 5:1429–1434. [PubMed: 16178252]
116. Nam KT, Kim DW, Yoo PJ, Chiang CY, Meethong N, Hammond PT, Chiang YM, Belcher AM. Virus-enabled synthesis and assembly of nanowires for lithium ion battery electrodes. Science. 2006; 312:885–888. [PubMed: 16601154]
117. Miura A, Tsukamoto R, Yoshii S, Yamashita I, Uraoka Y, Fuyuki T. Non-volatile flash memory with discrete bionanodot floating gate assembled by protein template. Nanotechnology. 2008; 19
118. Miura A, Uraoka Y, Fuyuki T, Yoshii S, Yamashita I. Floating nanodot gate memory fabrication with biomineralized nanodot as charge storage node. J Appl Phys. 2008; 103

119. Sano KI, Yoshii S, Yamashita I, Shiba K. In aqua structuralization of a three-dimensional configuration using biomolecules. Nano Lett. 2007; 7:3200–3202. [PubMed: 17824660]
120. Steinmetz NF, Bock E, Richter RP, Spatz JP, Lomonossoff GP, Evans DJ. Assembly of multilayer arrays of viral nanoparticles via biospecific recognition: A quartz crystal microbalance with dissipation monitoring study. Biomacromolecules. 2008; 9:456–462. [PubMed: 18197628]
121. Steinmetz NF, Calder G, Lomonossoff GP, Evans DJ. Plant viral capsids as nanobuilding blocks: Construction of arrays on solid supports. Langmuir. 2006; 22:10032–10037. [PubMed: 17106996]
122. Suci P, Klem MT, Young M, Douglas T. Signal ampflication using nanoplatform cluster formation. Soft Matter. 2008; 4:2519–2523.
123. Suci PA, Klem MT, Arce FT, Douglas T, Young M. Assembly of multilayer films incorporating a viral protein cage architecture. Langmuir. 2006; 22:8891–8896. [PubMed: 17014132]
124. Yoo PJ, Nam KT, Belchert AM, Hammond PT. Solvent-assisted patterning of polyelectrolyte multilayers and selective deposition of virus assemblies. Nano Letters. 2008; 8:1081–1089. [PubMed: 18355056]
125. Yoo PJ, Nam KT, Qi JF, Lee SK, Park J, Belcher AM, Hammond PT. Spontaneous assembly of viruses on multilayered polymer surfaces. Nature Materials. 2006; 5:234–240.
126. Gillitzer E, Willits D, Young M, Douglas T. Chemical modification of a viral cage for multivalent presentation. Chemical Communications. 2002:2390–2391. [PubMed: 12430455]
127. Kaltgrad E, O'Reilly MK, Liao LA, Han SF, Paulson JC, Finn MG. On-virus construction of polyvalent glycan ligands for cell-surface receptors. Journal of the American Chemical Society. 2008; 130:4578–4579. [PubMed: 18341338]
128. Kang S, Lander GC, Johnson JE, Prevelige PE. Development of bacteriophage P22 as a platform for molecular display: Genetic and chemical modifications of the procapsid exterior surface. Chembiochem. 2008; 9:514–518. [PubMed: 18213564]
129. Lewis JD, Destito G, Zijlstra A, Gonzalez MJ, Quigley JP, Manchester M, Stuhlmann H. Viral nanoparticles as tools for intravital vascular imaging. Nature Medicine. 2006; 12:354–360.
130. Miermont A, Barnhill H, Strable E, Lu XW, Wall KA, Wang Q, Finn MG, Huang XF. Cowpea mosaic virus capsid: A promising carrier for the development of carbohydrate based antitumor Vaccines. Chemistry-a European Journal. 2008; 14:4939–4947.
131. Prasuhn DE, Kuzelka J, Strable E, Udit AK, Cho SH, Lander GC, Quispe JD, Diers JR, Bocian DF, Potter C, Carragher B, Finn MG. Polyvalent display of heme on hepatitis B virus capsid protein through coordination to hexahistidine tags. Chemistry & Biology. 2008; 15:513–519. [PubMed: 18482703]
132. Strable E, Finn MG. Chemical Modification of Viruses and Virus-Like Particles. Current Topic in Microbiology and Immunology. 2009; 327:1–21.
133. Suci PA, Varpness Z, Gillitzer E, Douglas T, Young M. Targeting and photodynamic killing of a microbial pathogen using protein cage Architectures functionalized with a photosensitizer. Langmuir. 2007; 23:12280–12286. [PubMed: 17949022]
134. Wang Q, Lin T, Johnson JE, Finn MG. Natural supramolecular building blocks. Cysteine-added mutants of cowpea mosaic virus. Chemistry & Biology. 2002; 9:813–819. [PubMed: 12144925]
135. Berger S, Synytska A, Ionov L, Eichhorn KJ, Stamm M. Stimuli-Responsive Bicomponent Polymer Janus Particles by “Grafting from”/“Grafting to” Approaches. Macromolecules. 2008; 41:9669–9676.
136. Klem MT, Willits D, Young M, Douglas T. 2-D array formation of genetically engineered viral cages on Au surfaces and imaging by atomic force microscopy. Journal of the American Chemical Society. 2003; 125:10806–10807. [PubMed: 12952458]
137. Suci PA, Kang S, Young M, Douglas T. A Streptavidin-Protein Cage Janus Particle for Polarized Targeting and Modular Functionalization. Journal of the American Chemical Society. 2009; 131:9164–9165. [PubMed: 19522495]
138. Kang S, Suci PA, Broomell CC, Iwahori K, Kobayashi M, Yamashita I, Young M, Douglas T. Janus-like Protein Cages. Spatially Controlled Dual-Functional Surface Modifications of Protein Cages. Nano Letters. 2009; 9:2360–2366. [PubMed: 19441792]

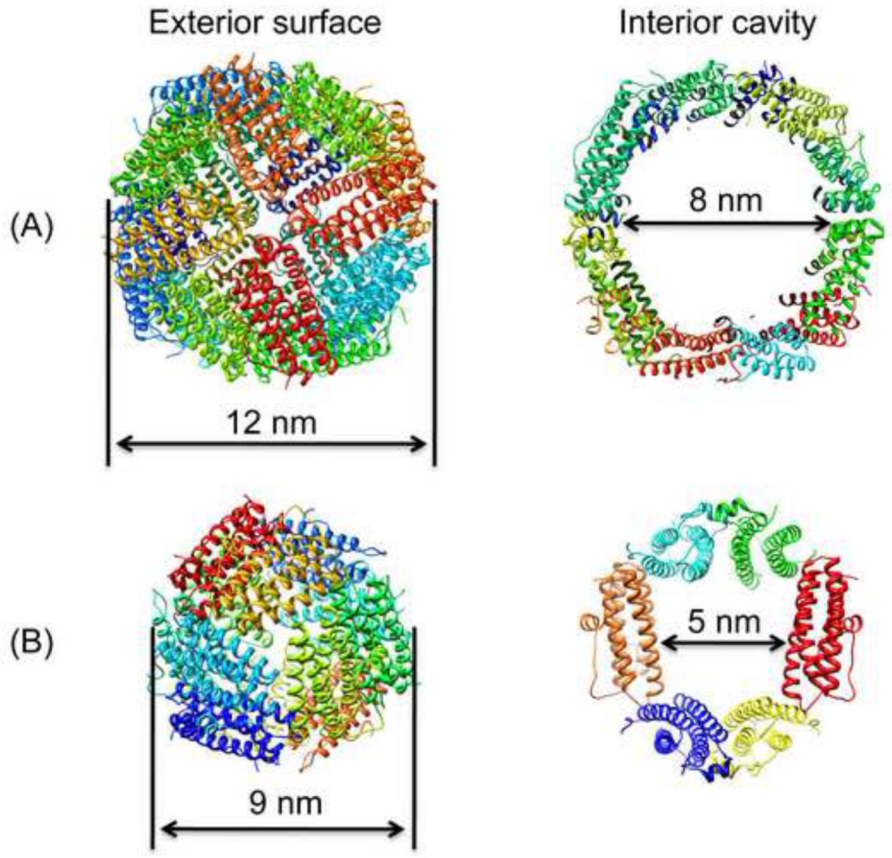

Fig. 1.
Ribbon diagrams of exterior surface view and interior cavity of (A) Human heavy-chain ferritin and (B) *Listeria innocua* Dps.

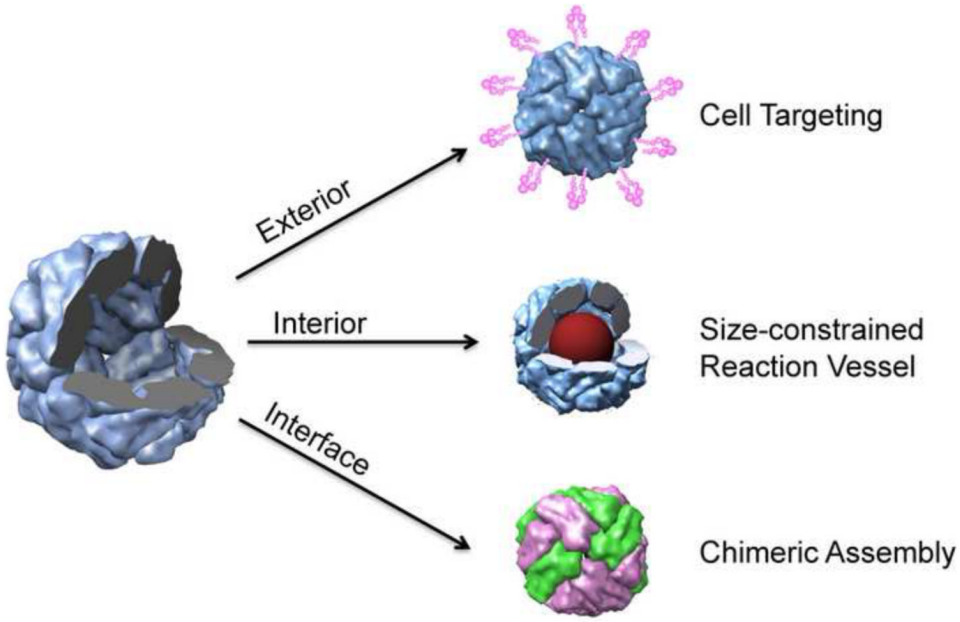

Fig. 2.
Schematic illustration of the three interfaces of a protein cages that can be exploited to impart designed functionalities.

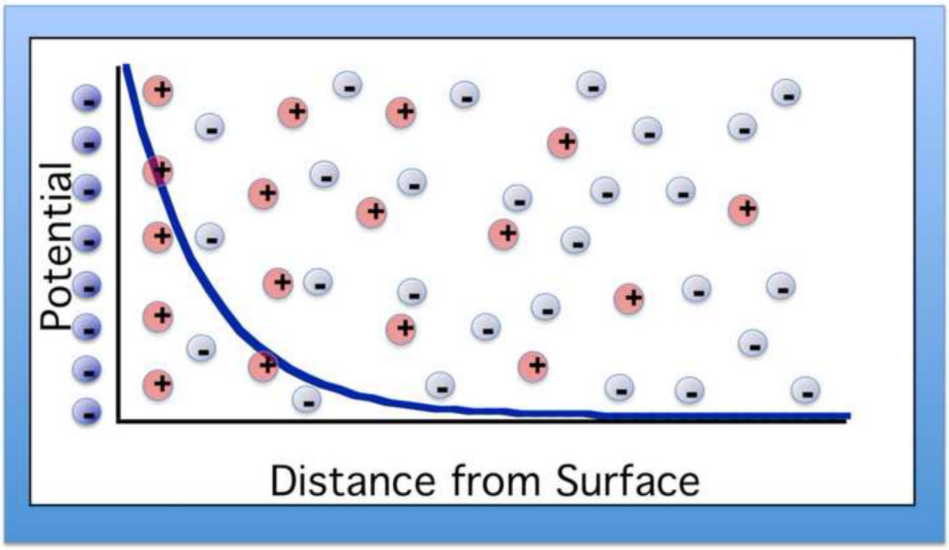

Fig. 3.
Schematic illustration of the ion distribution at a charged surface according to Gouy-Chapman theory. The electronic double layer is formed nearby the charged surface through Coulombic interactions.

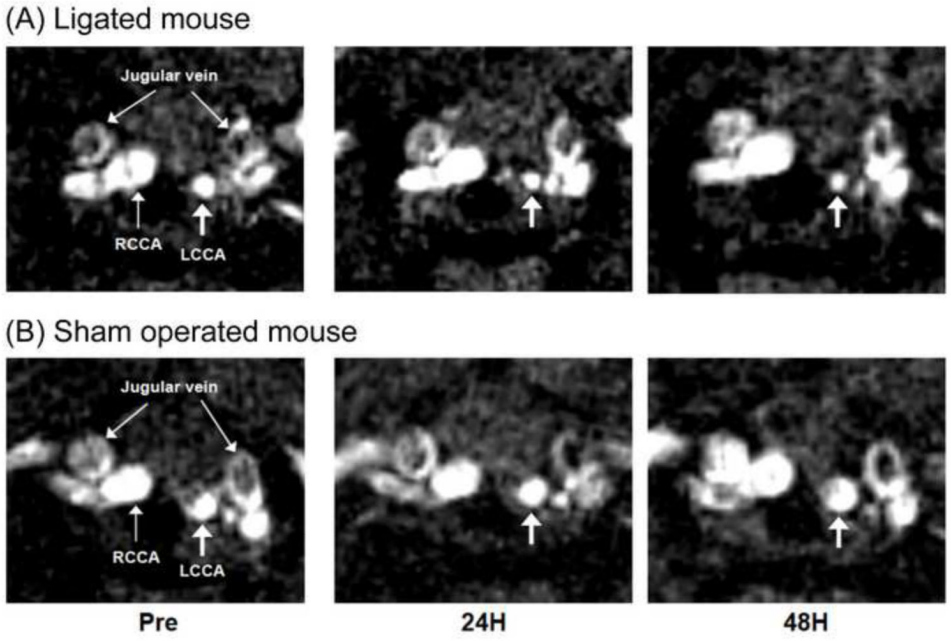

Fig. 4.

In vivo MRI of carotid arteries in (A) ligated mouse and (B) sham operated mouse; comparison of pre-injection, 24h and 48h post-injection of the mineralized HFn [80]. An atherosclerotic lesion was formed in left common carotid artery (LCCA) due to ligation of the artery but not formed either right common carotid artery (RCAA) of the same mouse or those arteries of the sham operated mouse. In the ligated mouse, concentric signal loss was observed around the LCCA lumen at 24 and 48 h post-injection of the mineralized HFn in comparison with pre-injection, but not the RCCA. No change was seen in either the LCCA or RCCA of sham operated mouse.

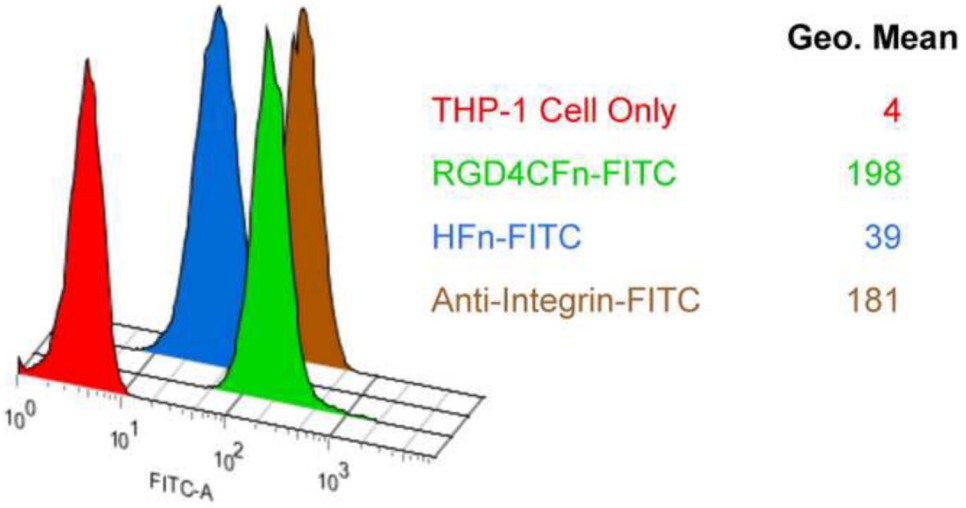

Fig. 5.

Fluorescence-activated cell sorting analysis of THP-1 cells incubated with fluorescently labeled RGD4C-Fn [86]. The data are plotted as histograms with their corresponding geometric (geo.) mean fluorescence values. Although the non-targeted protein cage (HFn) showed some interaction with the cells, the targeted cages (RGD4C-Fn) exhibit significantly increased interaction with the cells comparable to the positive control, anti-integrin $\alpha_v\beta_3$.

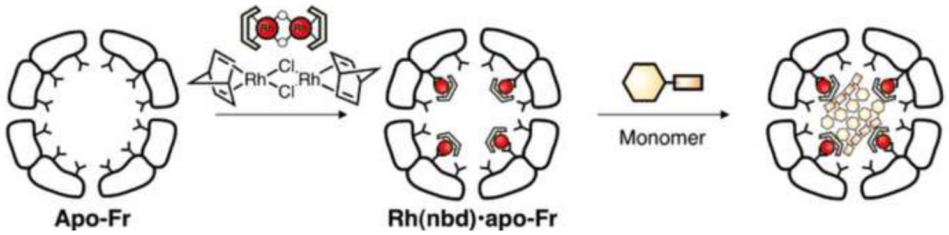

Fig. 6.

Schematic illustration of immobilization of $[Ru(nbd)Cl]_2$ complex into apo-Fn cage followed by polymerization of phenylacetylene catalyzed by the Fn [88]. The polymerization reaction occurs site-specifically inside of the Fn cage.

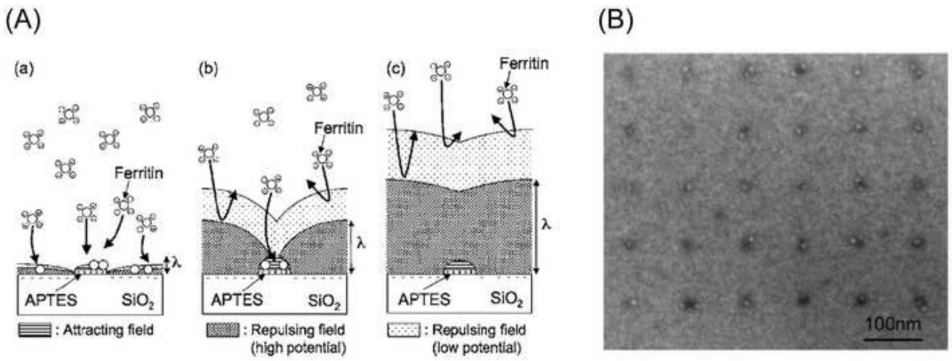

Fig. 7.

(A) Schematic illustration of ferritin adsorption onto a positively charged 3-aminopropyltriethoxysilane (APTES) nanodisc formed on a negatively charged SiO_2 substrate by an electrostatic interaction in solution under, (a) a short Debye length, λ, (b) a medium Debye length, and (c) a long Debye length. With a short λ, no selective adsorption onto the APTES area can be achieved because of short range interactions such as van der Waals force or hydrophobic interaction. With a long λ, ferritins can not reach to the APTES area due to the repulsive potential from the SiO_2 substrate. With an optimized λ, ferritins can be adsorbed only on the APTES area. (B) Single ferritin placement on APTES nanodisc patterns formed on an oxidized Si substrate. APTES disks of 15 nm diameter are prepared at 100 nm intervals on the substrate. Each APTES disk generally has one ferritin molecule. [97].

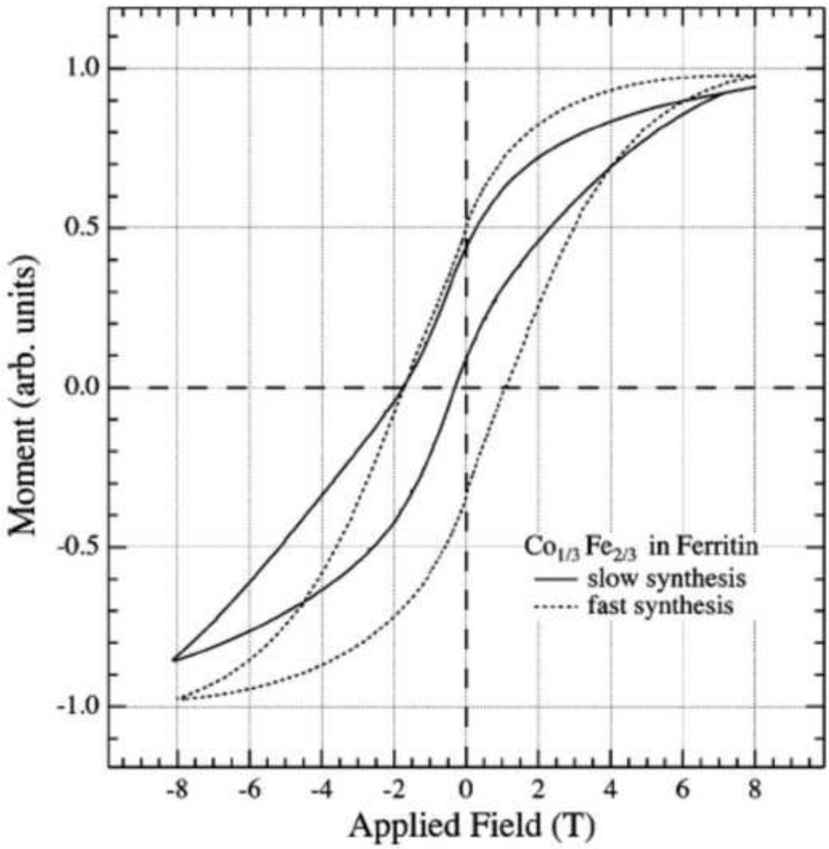

Fig. 8.

Hysteresis loops measured at 2 K for field-cooled (8T) mixed oxide material with nominal composition of 66% Fe_3O_4 and 33% Co_3O_4 prepared by slow (30 min) or fast (5 min) synthesis [104]. The offset between the two hysteresis loops is the exchange bias. The fast synthesis leads to Co incorporation as ferrimagnetic $Co_xFe_{3-x}O_4$ whereas slow synthesis results in a larger fraction of Co in antiferromagnetic Co_3O_4 which is available to bias the ferrimagnetic Fe_3O_4 present.

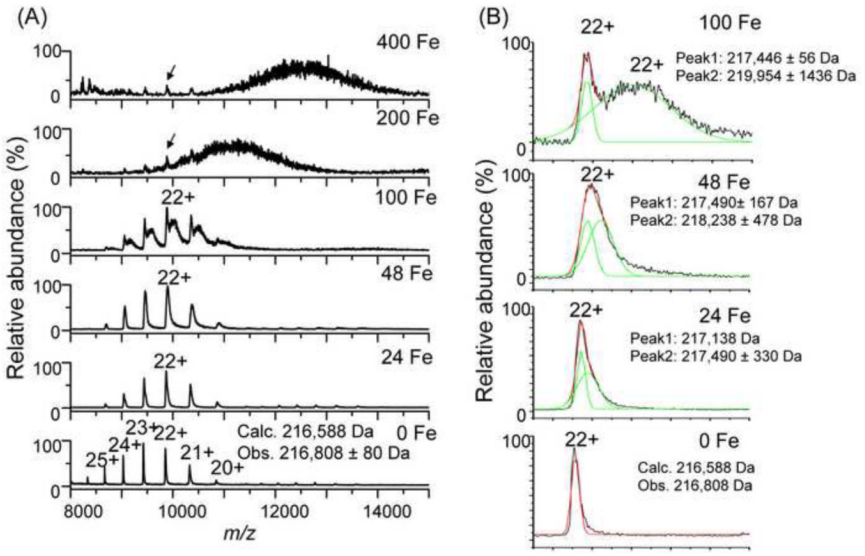

Fig. 9.

(A) Mass spectra of Fe-mineralized wild type LiDps at various loading factors of Fe(II). Charged peaks are indicated in the bottom spectrum [68]. (B) Fit (red line) of 22+ peaks of Fe-mineralized wt LiDps at lower loadings either with one or two Gaussians (green line). The peaks shift to higher m/z according to the increase of Fe^{2+} loading per cage indicates Fe_2O_3 particle growth in the cages. Fit of peaks demonstrates the presence of more than one mass distribution of the cages. The results allow us to establish a two-stage Fe_2O_3 particle growth process model[68].

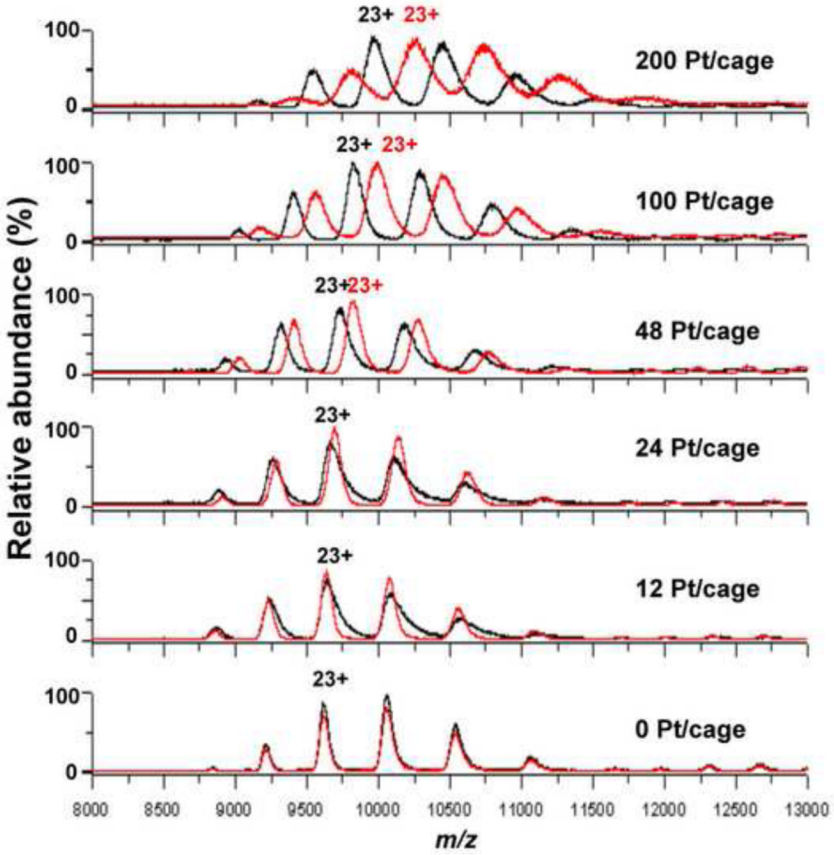

Fig. 10.

Overlaid mass spectra of the Pt^{2+} ion bound (black) and Pt^{0} mineralized (red) phen-S138C LisDps cages at various loading ratios of Pt^{2+} per cage. The charged peaks of 23+ of the cages are indicated [70]. The peaks shifted to higher m/z in accordance with increasing the number of Pt^{2+} ions loaded per cage.

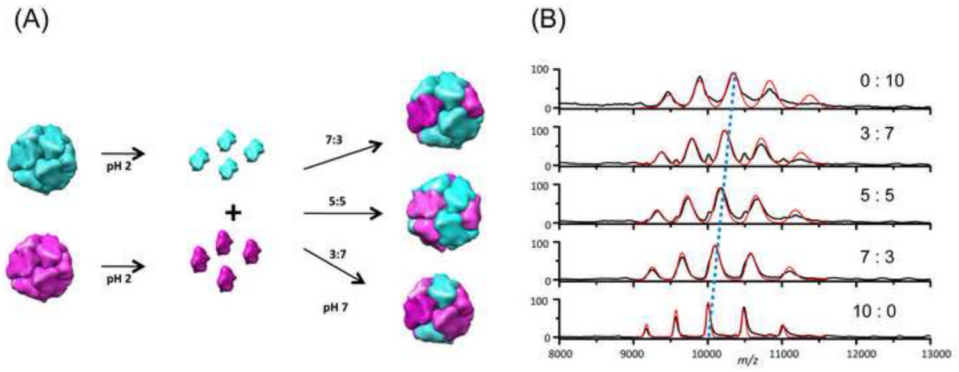

Fig. 11.

(A) Schematic representation of chimeric cage construction scheme. Two types of differentially modified S13C LiDps cages are disassembled to subunits at pH 2. Subsequently, the two types of subunits are mixed together with various ratios followed by reassembly to cages at pH 7. (B) Mass spectra of reassembled whole cages [110]. The peaks shift to higher m/z with increasing heavier subunit (blue subunits) ratio of the reassembled cages.

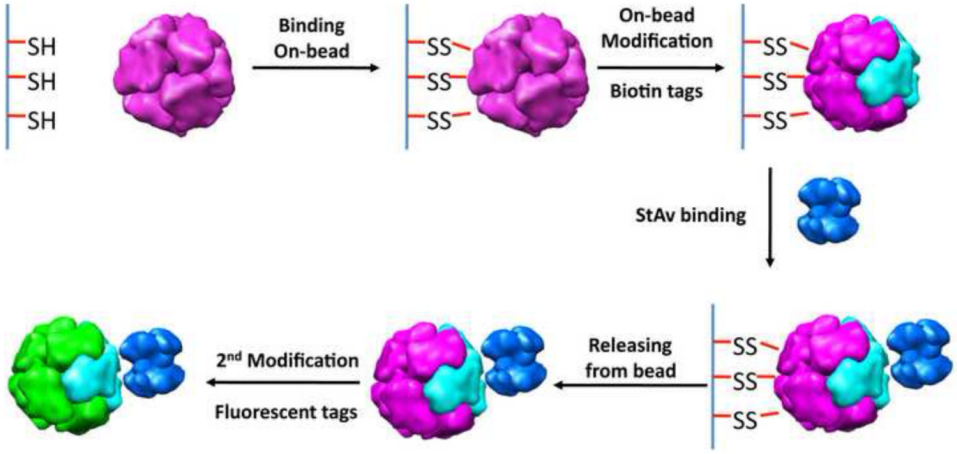

Fig. 12.

Schematic illustration of a Janus-like LiDps cage preparation scheme though a masking/unmasking technique on a solid bead support [138]. The protein cages are first immobilized on beads through disulfide bonds. The exposed sides of the protein cages are modified with maleimide-PEG_2-Biotin, which can selectively bind with streptavidin. Subsequently, the modified LiDps cages are eluted from the beads by reduction and the free cysteine residues on the cages are labeled with fluorescein-5-maleimide.